Folding analysis of the elastic ^{6}Li+^{12}C scattering: Knock-on exchange effects, energy dependence, and dynamical polarization potential

Dao T. Khoa,[1] G. R. Satchler,[2] and W. von Oertzen[1]
[1]*Bereich FK, Hahn-Meitner-Institut-GmbH, Glienicker Str. 100, D-14109 Berlin, Germany and Fachbereich Physik, Frei Universität Berlin, D-14195 Berlin, Germany*
[2]*Physics Division, Oak Ridge National Laboratory, Oak Ridge, Tennessee 37831*
(Received 1 December 1994)

Versions of the M3Y effective nucleon-nucleon interaction, with different prescriptions for the knock-on exchange contributions and density dependence, have been used in a study of the energy dependence of the nucleon optical potential in nuclear matter as well as in a systematic folding model analysis of the elastic ^{6}Li+^{12}C scattering data at $E_{\rm lab}$=60–318 MeV to study the energy dependence of the ^{6}Li+^{12}C optical potential. Contributions from the (breakup) dynamical polarization potential to the real part of the ^{6}Li+^{12}C optical potential are simulated by a surface correction using splines added to the real folded potential. This is shown to be strongest at $E_{\rm lab}$=99 MeV. The correction needed to fit the data is found to be qualitatively similar to that predicted theoretically for breakup of the ^{6}Li. The optical model analysis of the refractive ^{6}Li+^{12}C scattering data, using different types of real folded potential, shows that the most successful is the folded potential built upon density-dependent interactions, which have parameters chosen to reproduce the saturation properties of nuclear matter and which predict a nuclear incompressibility K around 200 MeV.

PACS number(s): 25.70.Bc, 24.10.Ht, 21.30.+y, 24.50.+g

I. INTRODUCTION

During the last two decades, the double-folding model [1] has been widely used to calculate the potential between two heavy ions (HI), due to its simple handling in numerical calculations. Usually, the optical model (OM) analysis of the HI scattering data is performed using the folded potential as the real part of the optical potential, while the imaginary potential is fitted in a phenomelogical form. Data on the scattering of light HI systems at large angles and high energies, such as those for ^{6}Li+^{12}C considered here, are particularly valuable. They are dominated by far-side scattering which in turn is sensitive to the nucleus-nucleus potential at small radii and not just at the surface [2]. Consequently, such data provide a stronger test of the validity of any model for HI potential (see, e.g., in Fig. 1 the decomposition of the elastic ^{6}Li+^{12}C scattering amplitude at different energies into the near- and far-side components using the method suggested by Fuller [3]).

The key inputs in a folding calculation are the nuclear densities of the colliding nuclei and the effective nucleon-nucleon (NN) interaction. For the latter, the M3Y interaction, based on the G-matrix elements of the Reid soft-core NN potential in an oscillator basis [4], is very popular. Due to uncertainties in the densities and the effective NN interaction, a slight renormalization of the folded potential to give the best fit to the data is a normally accepted procedure. If the deviation of the renormalization coefficient N_R from unity is small, this means success for the simple folding model [1]. However, it is well established that the folding analysis of the elastic ^{6}Li scattering requires a reduction of the N_R to about 0.6 [1,5]. This effect was shown by a complete coupled-channels reaction model [5] to be due to the breakup of the loosely bound ^{6}Li nucleus. The breakup effect can be represented by a dynamical polarization potential (DPP) which has a strongly repulsive real part in the surface, and an additional absorptive (imaginary) part [5]. This effect appears to remain important at energies up to at least $E/A \simeq 30$ MeV.

Recently, elastic ^{6}Li+^{12}C scattering at $E/A = 35$ and 53 MeV have been measured [6,7] and analyzed within the folding model. A surprising conclusion made in Ref. [7] is that *no renormalization* of the folded potential was necessary to reproduce the data at these energies, i.e., $N_R \simeq 1$. Since such a result might show that the breakup effect is totally absent at higher energies, it stimulated another folding analysis [8] of the same data using the original M3Y interaction [4]. It was found [8] that a reduction of N_R of about 30% is still needed to reproduce the data, and the result reported in Ref. [7] is mainly due to a different treatment of the knock-on exchange effects [9].

Nevertheless, it remains unclear which treatment of the exchange effects used in Refs. [8] and [7,9] is the most realistic one (although the authors of Ref. [9] already claim theirs to be so, based on an empirical comparison with the high-energy proton scattering data), and how strong the breakup effect is (namely, how strongly it might affect the real folded potential) at these higher energies. In the present work we apply a generalized version of the double-folding model [10], which takes into account the exchange and density-dependent effects as accurately as possible, to calculate the ^{6}Li+^{12}C potential for the OM analysis of the data at E/A ranging from 10 to 53 MeV. The folding calculation is first performed using the original density-independent M3Y interaction in

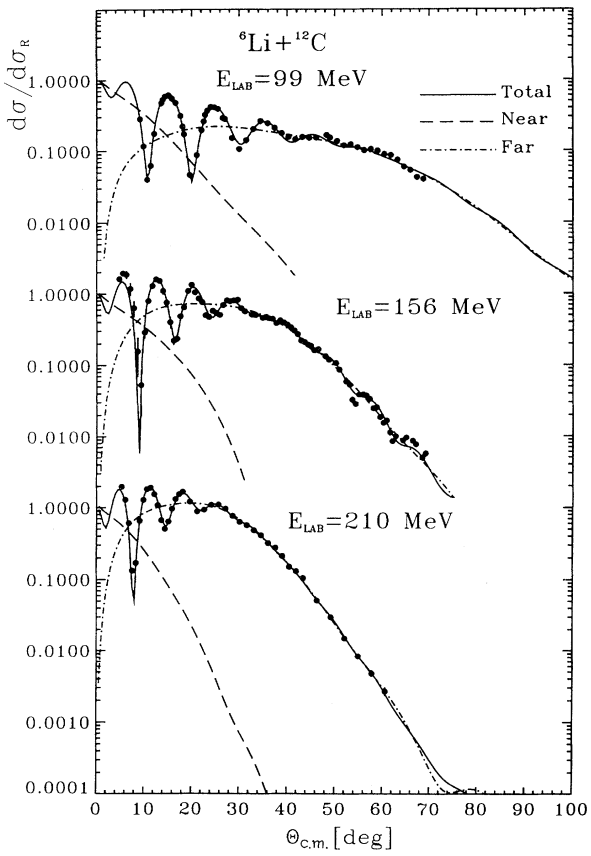

FIG. 1. Elastic ^{6}Li+^{12}C scattering cross sections at E/A = 16.5–35 MeV obtained with the BDM3Y1+spline real optical potential (see details in Sec. III C). The decomposition of the scattering amplitude into the near- and far-side components is done using the technique suggested in Ref. [3].

order to compare different treatments of the knock-on exchange effects, and to study the energy dependence of the ^{6}Li+^{12}C optical potential. The new density-dependent versions of the M3Y interaction [11], with the parameters chosen to reproduce the equilibrium density and binding energy of nuclear matter, are also used to calculate the ^{6}Li+^{12}C potential. For consistency, different interactions have also been used to study the energy dependence of the nucleon optical potential in a nuclear matter limit. Since the DPP contribution to the real part of the ^{6}Li+^{12}C optical potential has been shown to be strongest at the surface [5], its contributions to different real folded potentials are further simulated by a surface correction term constructed from splines. This method is shown to be more appropriate than the simple renormalization procedure ($N_R \neq 1$) to study the effects in the folded potential originating from different choices of the effective NN interaction.

II. THEORETICAL FORMALISM

A. M3Y effective interaction

To evaluate an in-medium NN interaction starting from a realistic free NN interaction still remains a challenge for the nuclear many-body theory. Therefore, most of the *microscopic* nuclear models still use different kinds of effective in-medium NN interaction. Among them, the M3Y interaction [4] has been used with some success in the folding model calculations of the HI optical potential (see, e.g., Ref. [1]). The original M3Y interaction was derived by fitting its matrix elements in an oscillator basis (with the oscillator parameters chosen to reproduce the ^{16}O ground state) to those elements of the G matrix obtained with the Reid soft-core NN interaction. Thus the medium modifications included are for some average over density and energy. The ranges of the M3Y forces were chosen to ensure a long-range (1.414 fm) tail of the one-pion-exchange potential (OPEP) as well as two short-range terms (0.25 and 0.4 fm) simulating the exchange of heavier mesons. The direct (v_D) and exchange (v_{EX}) parts of the central (spin-isospin independent) M3Y interaction have been determined from the singlet and triplet even ($v_{\rm SE}, v_{\rm TE}$) and odd ($v_{\rm SO}, v_{\rm TO}$) components of the two-nucleon force [4]

$$v_D(r) = 7999.0\frac{\exp(-4r)}{4r} - 2134.25\frac{\exp(-2.5r)}{2.5r}, \quad \text{(1a)}$$

$$v_{EX}(r) = 4631.38\frac{\exp(-4r)}{4r} - 1787.13\frac{\exp(-2.5r)}{2.5r} - 7.8474\frac{\exp(-0.7072r)}{0.7072r}. \quad \text{(1b)}$$

One can see from Eqs. (1) that the long-range OPEP is present only in the exchange part which makes the correct treatment of the knock-on exchange of nucleons between the projectile and the target very essential. Since the exact treatment of the knock-on exchange effects leads immediately to a nonlocal optical potential (see Sec. II B), various approximation schemes have been proposed. The simplest one is to replace (1b) by a zero-range, but energy-dependent, pseudopotential [12,13]. In this model, the central M3Y interaction is replaced by

$$v(r) = v_D(r) + \hat{J}_{00}(E)\delta(\mathbf{r}). \quad (2)$$

The energy-dependent strength $\hat{J}_{00}(E)$ has been determined empirically [12] by comparing proton scattering cross sections for different targets and energies, calculated using (2), with those calculated with the exact treatment of the exchange term of the proton-nucleus potential, using Eq. (1b). The results for nucleon energies up to about 80 MeV could be expressed [1] as

$$\hat{J}_{00}(E) \simeq -276[1 - 0.005(E/A)]\ \text{MeV fm}^3, \quad (3)$$

where A is the mass number of the projectile (A=1 for nucleons). In order to distinguish different treatments of the knock-on exchange effects, we denote the approximation (2) and (3) for the central M3Y interaction as the M3Y/PP1 interaction.

Another approach to the knock-on exchange effects, suggested in Refs. [7,9], is to parametrize the energy-dependent strength of the pseudopotential in a logarithmic form

$$\hat{J}_{00}(E) = -J^0_{00} + \beta \ln(6E/A), \quad (4)$$

with $J_{00}^0 \simeq 900$ MeV fm^3 and $\beta \simeq 140$ MeV fm^3. These two parameters were chosen [7,9] to reproduce the empirical energy dependence found for ^{6}Li scattering [6,7] as well as high energy proton and alpha scattering. It has been emphasized in Ref. [9] that the logarithmic energy dependence (4) is a more realistic representation of the knock-on exchange effects than the linear one (3). We refer to the prescription (2) and (4) for the central M3Y interaction as the M3Y/PP2 interaction. The two prescriptions give the same results at $E/A = 17$ MeV, when the two corresponding $\hat{J}_{00}(E)$ values are equal.

We note that of these two prescriptions for the zero-range pseudopotential, the M3Y/PP1 interaction has been widely used in different folding analyses. It could deliver, however, satisfying results only in cases where the HI interaction is dominated by strong absorption, i.e., when the scattering data are sensitive to the HI optical potential only in the surface region, and at energies neither too high ($E/A \leq 20$ MeV) nor too close to the Coulomb barrier where other polarization effects are expected to appear. In cases of nuclear rainbow scattering, observed first for α particles [14] and later on for other light HI systems (see, e.g., Refs. [15,16]), where the data are sensitive to the optical potential over a wider radial domain, the simple M3Y/PP1 interaction failed to give a good description of the data. In most cases the M3Y/PP1 folded potential turned out to be too deep at small internuclear distances which led to a wrong description of the rainbow (large-angle) region of the scattering cross section. Therefore, some further developments have been made to obtain a more realistic shape of the folded potential. One of these approaches is to impose on the original M3Y interaction an explicit density dependence, to account effectively for the in-medium effects which are more substantial at small distances (the so-called DDM3Y interaction [17]). Another way is to treat more correctly the single nucleon knock-on exchange effects [18,19], with the intrinsic energy and density dependence of the HI potential due to the exchange effects taken into account more accurately. In this approach the exchange potential is derived from first principles within a local density formalism, using the *finite-range* exchange interaction (1b), which is essentially a better approximation than the *zero-range* pseudopotential adopted in the M3Y/PP1 and M3Y/PP2 interactions. The local folded potential obtained in this method is referred to as the M3Y/FRE one. A systematic comparison of the M3Y/PP1 and M3Y/PP2 potentials with the M3Y/FRE potential should tell which of the two approximations (3) and (4) is the most realistic for the knock-on exchange effects.

Even though the M3Y/FRE and DDM3Y potentials have been successfully used to describe refractive α and HI scattering data, our recent nuclear matter study [11] using the M3Y interaction has shown that both the original M3Y interaction and its density-dependent version DDM3Y cannot provide a reasonable description of normal nuclear matter. Therefore, some different density dependences of the M3Y interaction have been introduced [11] which consistently reproduce the basic nuclear matter properties as well as the density and energy dependence of the nucleon optical potential. Namely, we have parametrized the energy- and density-dependent M3Y interaction in the form

$$v_{D(EX)}(\rho, E, r) = F(\rho) g(E) v_{D(EX)}(r), \quad \text{with } g(E) = 1 - 0.002E/A. \tag{5}$$

The explicit form of the density-dependent factor $F(\rho)$ is given by Eqs. (3) and Table I of Ref. [10]. The new density-dependent M3Y interactions have been used successfully to calculate the nucleus-nucleus potential (with the *local* exchange part evaluated exactly, in the same way as for the M3Y/FRE potential) and applied to the analysis [10,20] of the refractive scattering of α particles, ^{12}C, and ^{16}O. In the present work these new density-dependent interactions are also used to calculate the ^{6}Li+^{12}C potential for the folding analysis of the considered scattering data.

B. Generalized double-folding model

We give here only a short summary of the generalized version of the folding model and refer to Ref. [10] for more details. In the first order of the many-body theory, the microscopic nucleus-nucleus potential is evaluated as an antisymmetrized Hartree-Fock-type potential of the dinuclear system

$$V = V_D + V_{EX} = \sum_{i \in A_1, j \in A_2} [\langle ij|v_D|ij\rangle + \langle ij|v_{EX}|ji\rangle], \tag{6}$$

where $|i\rangle$ and $|j\rangle$ refer to the single-particle wave functions of nucleons in the two colliding nuclei A_1 and A_2, respectively; v_D and v_{EX} are the direct and exchange parts [Eqs. (1)] of the effective NN interaction. The exchange potential V_{EX} accounts for the knock-on exchange of nucleons between the projectile and the target. By introducing one-body density matrices $\rho_{1(2)}(\mathbf{r}, \mathbf{r}')$ of the two colliding nuclei [with $\rho(\mathbf{r}, \mathbf{r}) \equiv \rho(\mathbf{r})$], one can explicitly write the energy-dependent direct and exchange potentials as

$$V_D(E, \mathbf{R}) = \int \rho_1(\mathbf{r}_1)\rho_2(\mathbf{r}_2) v_D(\rho, E, s) d^3r_1 d^3r_2, \quad \mathbf{s} = \mathbf{r}_2 - \mathbf{r}_1 + \mathbf{R}, \tag{7}$$

$$V_{EX}(E, \mathbf{R}) = \int \rho_1(\mathbf{r}_1, \mathbf{r}_1 + \mathbf{s})\rho_2(\mathbf{r}_2, \mathbf{r}_2 - \mathbf{s}) v_{EX}(\rho, E, s) \times \exp\left[\frac{i\mathbf{k}(\mathbf{R}) \cdot \mathbf{s}}{M}\right] d^3r_1 d^3r_2. \tag{8}$$

Here $k(\mathbf{R})$ is the relative-motion momentum given by

$$k^2(\mathbf{R}) = \frac{2mM}{\hbar^2}[E_{\text{c.m.}} - V(E, \mathbf{R}) - V_C(\mathbf{R})], \tag{9}$$

where $M = A_1A_2/(A_1+A_2)$ is the reduced mass number, $E_{\text{c.m.}}$ is the center-of-mass (c.m.) energy, and m is the bare nucleon mass. $V(E, \mathbf{R}) = V_D(E, \mathbf{R}) + V_{EX}(E, \mathbf{R})$ and $V_C(\mathbf{R})$ are the total nuclear and Coulomb potentials,

respectively. The folded potential V is *nonlocal* through its exchange term and contains a self-consistency problem because k depends upon V. The exact treatment of the nonlocal exchange term is complicated numerically, but one may obtain an equivalent *local* potential by using a realistic approximation for the mixed density matrix [21]

$$\rho(\mathbf{R},\mathbf{R}+\mathbf{s}) \simeq \rho\left(\mathbf{R}+\frac{\mathbf{s}}{2}\right)\hat{j_1}\left(k_F\left(\mathbf{R}+\frac{\mathbf{s}}{2}\right)s\right)$$

$$\text{with} \quad \hat{j_1}(x) = 3(\sin x - x\cos x)/x^3. \tag{10}$$

The average local Fermi momentum k_F is chosen [21] to accelerate the convergence of the density-matrix expansion. Its explicit form is given in Ref. [10].

We note that the procedure (7)–(10) is developed for the folding calculation using the energy- and density-dependent interaction (5). The overlap density which enters Eq. (5) is taken to be the sum of the densities of the two colliding nuclei at the midpoint of the internucleon separation

$$F(\rho) = F\left(\rho_1\left(\mathbf{r}_1+\frac{\mathbf{s}}{2}\right)+\rho_2\left(\mathbf{r}_2-\frac{\mathbf{s}}{2}\right)\right). \tag{11}$$

This is the so-called frozen density approximation, usually adopted in the folding-model calculation [1,10,17,22]. After certain transformations one obtains the self-consistent and local exchange potential V_{EX} as

$$\begin{aligned} V_{EX}(E,\mathbf{R}) = 4\pi g(E)\int_0^\infty v_{EX}(s)s^2 ds\, j_0(k(\mathbf{R})s/M) \\ \times \int f_1(\mathbf{r},s) f_2(\mathbf{r}-\mathbf{R},s) \\ \times F(\rho_1(\mathbf{r})+\rho_2(\mathbf{r}-\mathbf{R}))d^3r, \end{aligned} \tag{12}$$

where

$$f_{1(2)}(\mathbf{r},s) = \rho_{1(2)}(\mathbf{r})\hat{j_1}(k_{F1(2)}(\mathbf{r})s)$$

and

$$j_0(x) = \sin x/x.$$

The exchange potential (12) can then be evaluated exactly by an iterative method [10]. Then the calculated total potential $V(E,R)$ has an energy dependence arising from the exchange term [see Eqs. (8) and (9)]. At the energies considered in the present study, this exchange energy dependence is roughly twice as great as the intrinsic dependence represented by the $g(E)$ factor. Consequently, to have a realistic energy dependence of the folded potential, one should treat the knock-on exchange effects as accurately as possible.

To calculate the M3Y/FRE potential using the energy- and density-*independent* interaction (1a) and (1b) one needs to evaluate the direct and exchange potentials (7) and (8) using the same procedure but putting $F(\rho) = g(E) \equiv 1$. The calculation of the M3Y/PP1 and M3Y/PP2 potentials is simply reduced to the calculation of the six-dimensional integral (7) with $v_D(r)$ being replaced by the interaction (2), using the prescriptions (3) and (4) for the pseudopotential, respectively. Thus the energy dependence of the M3Y/PP1 or M3Y/PP2 potential is determined explicitly by the empirical relation (3) or (4), while the energy dependence of the M3Y/FRE potential comes out entirely from the evaluation of the exchange potential (8).

A useful quantity in the study of the energy dependence is the volume integral of the folded potential per interacting nucleon pair

$$\begin{aligned} J_R(E)/(A_1A_2) \\ = \frac{4\pi}{A_1A_2}\int_0^\infty [V_D(E,r)+V_{EX}(E,r)]\,r^2dr. \end{aligned} \tag{13}$$

Due to the zero range of the pseudopotential used in (3) and (4) the J_R values for the M3Y/PP1 and M3Y/PP2 potentials are simply

$$J_R(E)/(A_1A_2) = J_D + \hat{J}_{00}(E), \tag{13'}$$

where the volume integral of the direct part $J_D = -145.9$ MeV fm^3. In other cases the integration has to be performed separately at each energy to obtain the J_R/A_1A_2 value.

The nuclear densities used in our folding calculation are constructed using the shell model [23] for the considered nuclei. Since the original M3Y interaction (1) is real, the folded potentials enter the OM analyses as the real part of the optical potential. The imaginary part is taken to have a conventional Woods-Saxon (WS) form. Thus the ^{6}Li+^{12}C optical potential is

$$U(E,R) = N_R[V_D(E,R)+V_{EX}(E,R)] + iW(R), \tag{14}$$

with

$$W(R) = -W_V\left\{1+\exp\left[\frac{R-r_V(6^{1/3}+12^{1/3})}{a_V}\right]\right\}^{-1}, \tag{15}$$

where the renormalization factor N_R together with WS parameters W_V, r_V, and a_V are adjusted for the best fit to the data. The Coulomb potential $V_C(R)$ used in the calculation of the exchange potential [see Eq. (9)] and in the OM analysis is generated by folding two uniform charge distributions with radii of 3.22 and 3.17 fm for ^{6}Li and ^{12}C, respectively. All the OM analyses were made using the code PTOLEMY [24].

The breakup effect in the ^{6}Li+^{12}C system can be represented by a dynamical polarization potential [5] whose real part is expected to be repulsive and peaked at the surface. This contribution from the DPP is simulated in our folding analysis by a surface correction term $\Delta V(R)$ added to the real folded potential. Then the optical potential becomes

$$U(E,R) = V_D(E,R)+V_{EX}(E,R)+\Delta V(R)+iW(R), \tag{16}$$

where the shape of $\Delta V(R)$ is defined by its values at certain radial knots with a cubic spline interpolation be-

tween the knots. The $\Delta V(R)$ values at the knots are parameters adjusted to fit the scattering data. Although in such a "folding+spline" analysis there are more free parameters, the results should be more significant than those obtained in a folding analysis where the contribution from the DPP is taken into account simply by renormalizing the folded potential as a whole. The volume integrals (13) have to be renormalized by N_R or have contribution from ΔV added, depending on which of the two schemes (14) and (16) is used in the OM analysis.

III. RESULTS AND DISCUSSIONS

A. Energy dependence of the nucleon optical potential

We shall find below that, within the folding model, more than one half of the energy dependence of the HI potential comes from the exchange term (see Sec. II B). The remainder comes from an intrinsic energy dependence of the effective interaction which has been approximated by the energy dependence (5). One finds a similar behavior for the nucleon optical potential [11], and it was this study that led to the introduction of the energy dependent factor $g(E)$ in Eq. (5). We have calculated the nucleon optical potential at nucleon incident energies up to 200 MeV using various M3Y interactions. In the nuclear matter limit, the nucleon optical potential is determined as the interaction potential between the incident nucleon and those in the filled Fermi sea. Applying a *continuous choice* for the nucleon single-particle potential [25] at positive energies, the following expression can be obtained [11] for the nucleon optical potential using the central (spin-isospin independent) M3Y interaction (1)

$$U(\rho,E)=\rho\left[J_D+\int j_0(kr)\hat{j}_1(k_Fr)v_{EX}(r)d^3r\right], \quad (17)$$

where $J_D=-145.9$ MeV fm^3, k is the nucleon momentum ($k>k_F$) and is related to the incident energy E as

$$k=\sqrt{\frac{2m}{\hbar^2}[E-U(\rho,E)]}. \quad (18)$$

We note that the exchange term in Eq. (17) is evaluated *exactly* in this nuclear matter case since the incident nucleon has been antisymmetrized with all other nucleons in the medium (with $k'\le k_F$). This leads to a self-consistency problem in evaluating $U(\rho,E)$. We have used a simple iteration method to calculate $U(\rho,E)$, and the results are shown in Fig. 2 as the M3Y/FRE curve.

For the M3Y/PP1 and M3Y/PP2 interactions the calculation of $U(\rho,E)$ is simplified by the zero-range prescription for the exchange part, and one has

$$U(\rho,E)=\rho[J_D+\hat{J}_{00}(E)]. \quad (19)$$

The results obtained using prescription (3) or (4) for $\hat{J}_{00}(E)$ are shown in Fig. 2 as the M3Y/PP1 or M3Y/PP2 curve, respectively. As in the case of the M3Y/FRE interaction, the energy dependence of $U(\rho,E)$ obtained with the M3Y/PP1 or M3Y/PP2 interaction arises entirely from the exchange term.

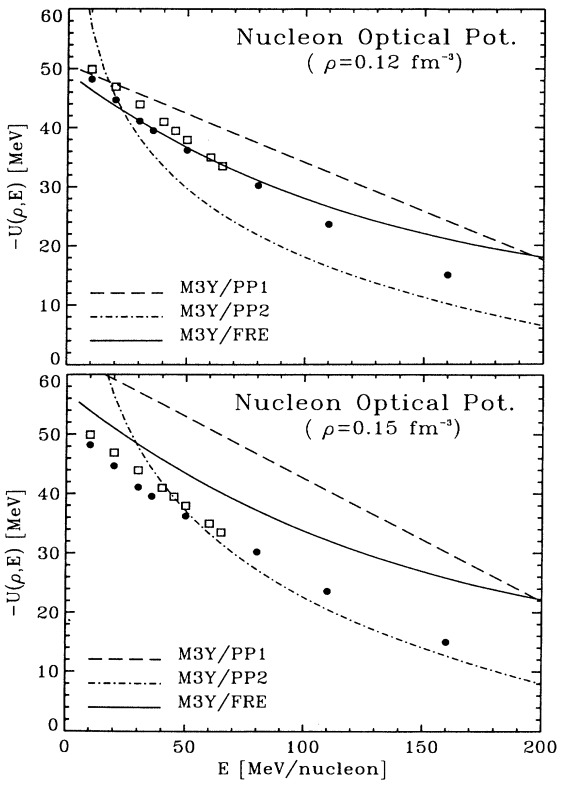

FIG. 2. Energy dependence of the nucleon optical potential evaluated at different nuclear matter densities using the M3Y/PP1, M3Y/PP2, and M3Y/FRE prescriptions for the knock-on exchange effects. The full circles and open squares are the empirical data taken from Refs. [26] and [27], respectively.

For the energy- and density-dependent interactions (5) the $U(\rho,E)$ is calculated by the same method, but with the energy- and density-dependent factors taken into account during the iteration, i.e.,

$$U(\rho,E)=F(\rho)g(E)\rho\left[J_D+\int j_0(kr)\hat{j}_1(k_Fr)v_{EX}(r)d^3r\right]. \quad (17')$$

In Figs. 2 and 3 we show $U(\rho,E)$ evaluated for ρ close to the normal nuclear matter density compared with the empirical values [26,27]. From the discussion above it is clear that the curves M3Y/PP1 and M3Y/PP2 are just two different approximations to the exact M3Y/FRE result. One can see from Fig. 2 that the linear M3Y/PP1 result is closer to the exact result while the logarithmic dependence (4) gives the M3Y/PP2 potential much more attractive at low energies and less attractive at high energies compared to the exact M3Y/FRE potential. The slope of the M3Y/PP1 and M3Y/FRE potentials is in a

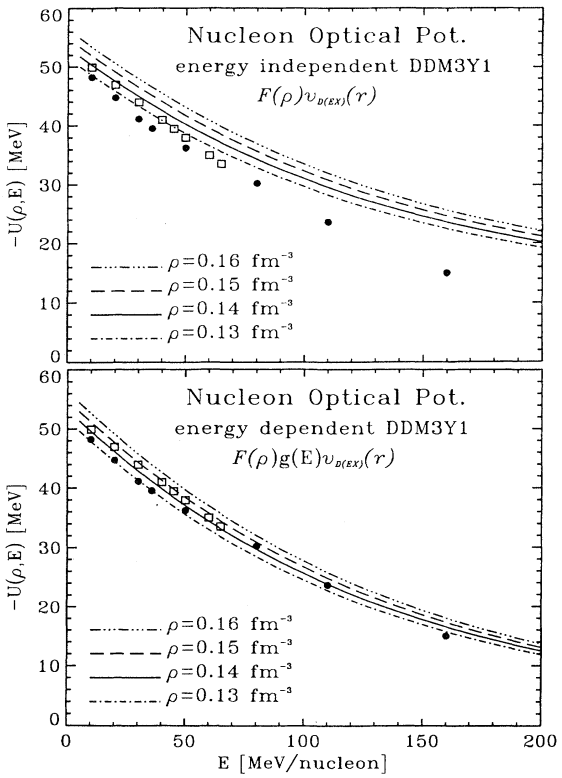

FIG. 3. The same as Fig. 2 using the energy-independent (upper part) and energy-dependent (lower part) DDM3Y1 interaction, with the exact treatment of the knock-on exchange effects.

good agreement with that of the empirical data at low energies. With increasing energy, the calculated M3Y/FRE potential is somewhat more attractive than the empirical one. The logarithmic formula (4) leads to a wrong slope of the M3Y/PP2 potential at energies up to about 50 MeV. At higher energies the slope of the M3Y/PP2 potential begins, as expected, to approach that of the empirical data.

The density-*independent* M3Y interaction (1), as noted above, is not able to reproduce the saturation properties of normal nuclear matter [11]. This necessitated the introduction of a realistic density dependence [see Eq. (5)] to the M3Y interaction. To show the effects of the density dependence in the nucleon optical potential we have calculated $U(\rho, E)$ using the density-dependent DDM3Y1 interaction [11] but without the energy-dependent factor $g(E)$, i.e., by putting $g(E) \equiv 1$ in Eq. (17′). The results are shown in the upper part of Fig. 3, and one finds that the calculated $U(\rho, E)$ is a bit less attractive compared with the M3Y/FRE result, but the slope remains almost the same. This effect is easily understood in light of the microscopic results for the nucleon optical potential [25], where the energy dependence was shown to come not only from the exchange part but also from the direct part of the Brueckner G matrix. That is the reason why an additional energy dependence has been introduced into the interaction (5), in terms of the $g(E)$ factor. In the lower part of Fig. 3 we show the results obtained with the energy-dependent DDM3Y1 interaction [$g(E) \neq 1$], and one can see a good agreement with the empirical values at all energies. The best fit is given by the nucleon optical potential evaluated at $\rho \leq 0.14$ fm^{-3}. This is natural since the elastic nucleon scattering occurs not in the deepest interior but rather in outer regions of the target. Thus the intrinsic energy dependence $g(E)$ in Eq. (5) is found to be appropriate for either the BDM3Y1 or DDM3Y1 versions of the interaction.

B. Folding analysis of the ^{6}Li+^{12}C scattering and the energy dependence of the real optical potential

Different treatments of the knock-on exchange effects lead to similar differences in the calculated ^{6}Li+^{12}C potentials. We have first used different M3Y interactions to evaluate the energy dependent volume integral (13) of the ^{6}Li+^{12}C folded potentials at energies up to $E/A = 80$ MeV. The results shown in Fig. 4 are also compared with an "empirical" energy dependence (solid curve) of the $J_R/6A$ value suggested in a logarithmic form by the authors of Refs. [6,7,9]

$$J_R/6A = -J_R^0/(6A) + \beta_R \ln(6E/A), \qquad (20)$$

with $J_R^0 \simeq 830$ MeV fm^3 and $\beta_R \simeq 100$ MeV fm^3. Since the parameters in Eq. (4) were actually chosen [7,9] to give an energy dependence of the folded M3Y/PP2 potential close to Eq. (20), one finds from Fig. 4 that the M3Y/PP2 curve is quite close to the empirical one. As in the case of the nucleon optical potential, the $J_R/6A$ values of the M3Y/PP1 potential agree well with those of the M3Y/FRE potential. This again indicates that the prescription (3) for the pseudopotential in Eq. (2) is a better representation of the knock-on exchange effects than is the prescription (4). The result obtained with the energy- and density-dependent DDM3Y1 interaction are less attractive than those given by the M3Y/PP1 and

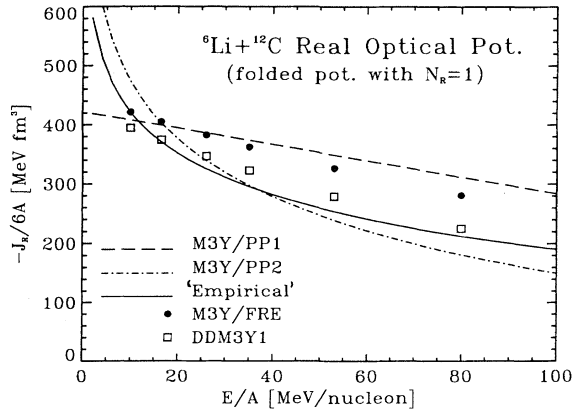

FIG. 4. Energy dependence of the volume integral (13) per interacting nucleon pair $J_R/6A$ of the real (unrenormalized) ^{6}Li+^{12}C folded potentials obtained with the M3Y/PP1, M3Y/PP2, M3Y/FRE, and DDM3Y1 interactions. The solid curve is the "empirical" logarithmic dependence suggested in Refs. [6,7,9].

M3Y/FRE interactions and also closer to the empirical results. However, its slope at low energies is different from the logarithmic dependence (20). It is also shown below that the behavior of the realistic $J_R/6A$ values derived from the best fit to the whole set of data is quite different from the logarithmic law at low energies.

The difference found in the $J_R/6A$ values for different potentials is reflected in the radial shape of the folded potentials. In Fig. 5 we plotted the folded potentials obtained with different interactions for the ^{6}Li+^{12}C system at $E/A = 10$ and 35 MeV. The M3Y/PP2 potential is much deeper at $E/A = 10$ MeV but becomes much shallower at $E/A = 35$ MeV than the M3Y/PP1 and M3Y/FRE potentials. The M3Y/PP1 potential is always deeper than the M3Y/FRE potential in the center, an effect shown [18,19] to be due to the inadequacy of the pseudopotential approximation for the exchange term. With both the exchange and density-dependent effects more accurately taken into account, the DDM3Y1 folded potential becomes less attractive at small radii than the M3Y/PP1 and M3Y/FRE potentials. The difference between the M3Y/PP2 and DDM3Y1 potentials is very large at low energies, but becomes smaller as the energy increases.

These folded potentials were used in the OM analysis of the elastic ^{6}Li+^{12}C scattering at $E_{\rm lab} = 60$ [28], 99 [29], 156 [30], 210 [6], and 318 MeV [7], using the prescription (14). In Figs. 6–9 and Table I the results given by the density-dependent DDM3Y1 and BDM3Y1 interactions [10,11] are compared with those given by the density-independent M3Y/PP1, M3Y/PP2, and M3Y/FRE interactions. We emphasize that the exchange parts of the DDM3Y1, BDM3Y1, and M3Y/FRE potentials are calculated using the same method, with the finite-range exchange interaction (1b). As in previous OM analyses of these data, no spin-orbit potential was included in our OM calculation since the weak spin-orbit interaction for ^{6}Li has been shown [31] to have little influence on the elastic scattering cross section. Except at $E/A = 10$ MeV, the ^{6}Li+^{12}C scattering data show strong refractive effects where the near- and far-side interference pattern in the angular distribution is followed by a smooth rainbow pattern dominated by the refraction of the far-side amplitude (see Fig. 1). We further recall that the refractive scattering pattern is very sensitive to the real optical potential at small radii [2]. Therefore, the shape of the measured angular distribution at large angles is essential to test different types of the (real) folded potential.

From the results shown in Figs. 6–8 one finds that different folded potentials, after being properly renormalized to optimize the fit to the data (see Table I and Fig. 9), give slightly different descriptions of the elastic scattering data. Since a strong renormalization of the real folded potential has been shown to be caused by the

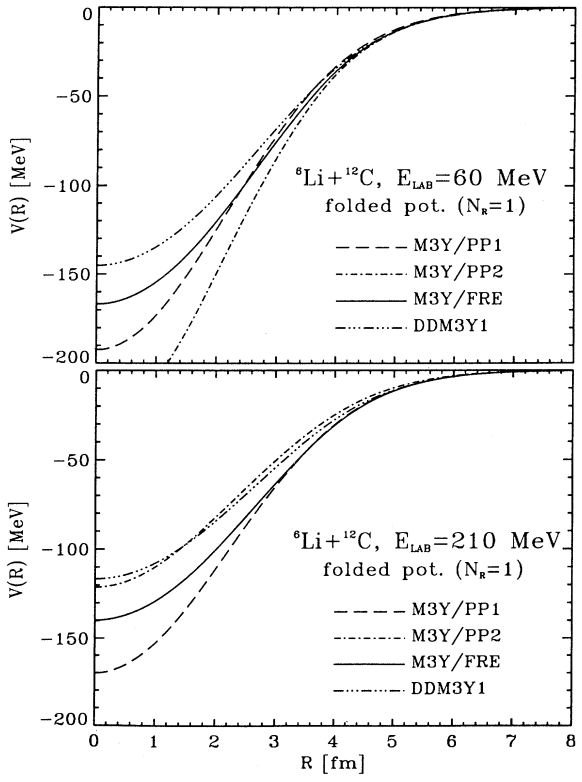

FIG. 5. Real (unrenormalized) ^{6}Li+^{12}C folded potential obtained with the M3Y/PP1, M3Y/PP2, M3Y/FRE, and DDM3Y1 interactions at $E/A = 10$ and 35 MeV.

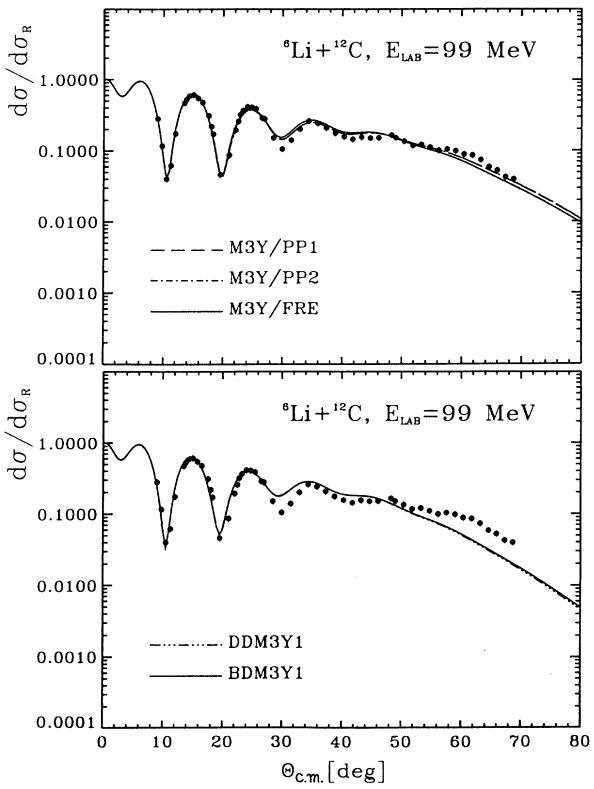

FIG. 6. OM fits to the elastic ^{6}Li+^{12}C scattering data at $E/A = 16.5$ MeV given by the renormalized M3Y/PP1, M3Y/PP2, M3Y/FRE (upper part), and DDM3Y1, BDM3Y1 (lower part) folded potentials. The corresponding OM parameters are given in Table I.

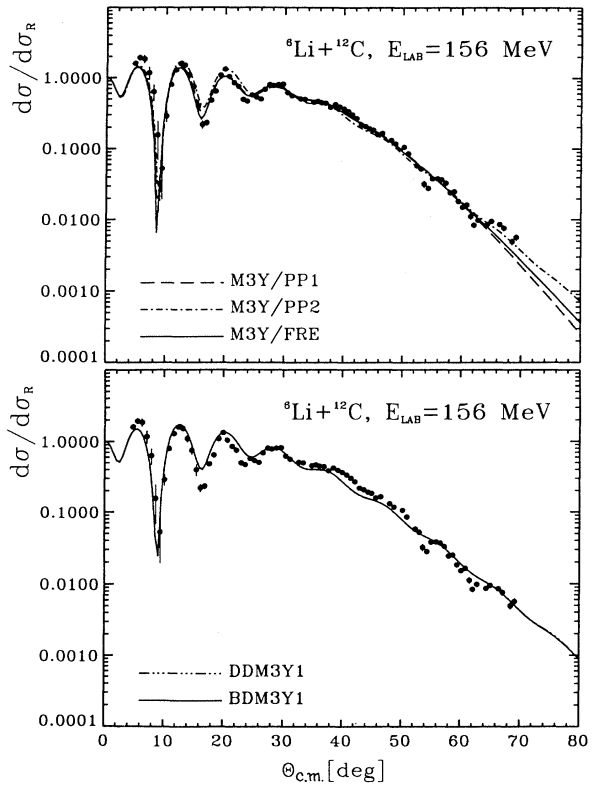

FIG. 7. The same as Fig. 6 but at $E/A = 26$ MeV.

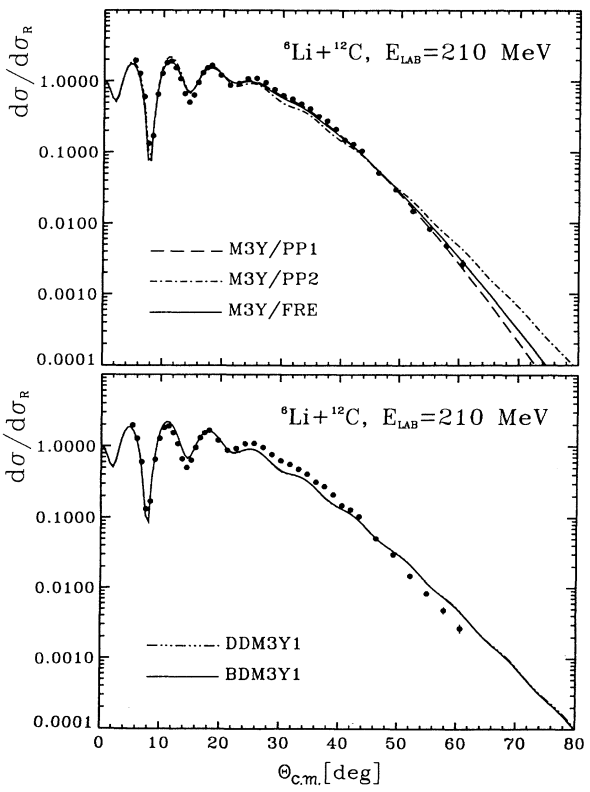

FIG. 8. The same as Fig. 6 but at $E/A = 35$ MeV.

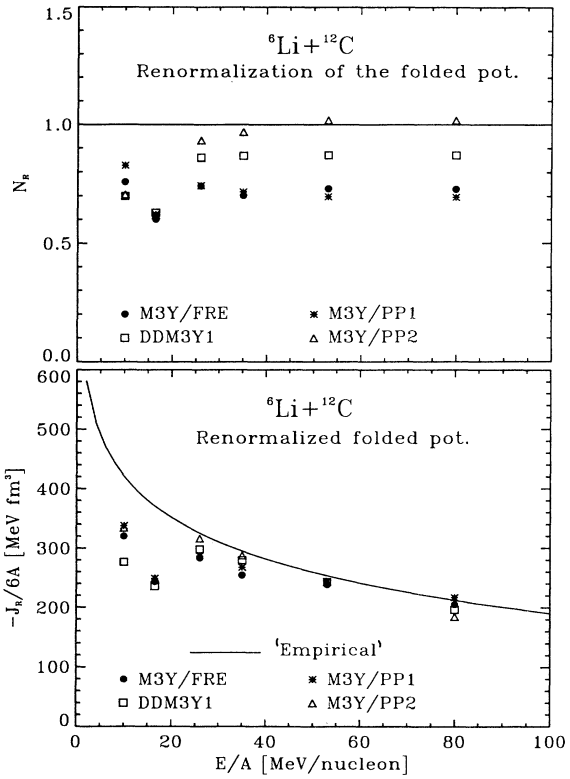

FIG. 9. Energy dependence of the volume integral (13) per interacting nucleon pair $J_R/6A$ of different real ^{6}Li+^{12}C folded potentials (lower part) renormalized by the corresponding N_R factors (upper part). The N_R factors at $E/A = 80$ MeV are taken the same as found at $E/A = 53$ MeV. The solid $J_R/6A$ curve is the "empirical" logarithmic dependence suggested in Refs. [6,7,9].

breakup effect [5], different energy dependences of the N_R factor obtained with different types of the folded potential (Fig. 9) raises some question about the energy dependence of the breakup effect in the elastic ^{6}Li+^{12}C scattering. In the complete coupled-channels calculation by Sakuragi [5], the M3Y/PP1 folded potential was used for both the real and imaginary potentials (with $N_R = 1$ and N_I adjusted to fit the data). From these results, which certainly depend on the choice of the folded potential, one finds that the breakup effect depends little on the energy (at E/A up to about 28 MeV) and the corresponding DPP has a repulsive real part peaked at the surface, with a strength there of about 30–40% of the M3Y/PP1 potential. In our folding analysis, the M3Y/PP1 and M3Y/FRE potentials have about the same N_R at different energies (upper part of Fig. 9) and require a renormalization of at least 30% up to $E/A = 53$ MeV which, according to Sakuragi's results, might indicate a strong breakup effect also at higher energies. The M3Y/PP2 potential, calculated with a different prescription for the knock-on exchange effects, has N_R approaching unity already at $E/A = 26$ and 35 MeV, and one might expect that the coupled-channels calculation using this potential

would show a disappearance of the DPP at high energies [7,9].

Finally, the density-dependent DDM3Y1 and BDM3Y1 potentials have N_R approaching the "standard" value of about 0.9 obtained from our previous folding analysis [10] of the ^{12}C and ^{16}O scattering data, already at $E/A = 26$ MeV. However different the N_R values for different folded potentials are, they all tend to give about the same $J_R/6A$ value (lower part of Fig. 9). These values seem to approach the "empirical" curve (20) at high energies, while differing strongly from it at $E/A = 10$ and 16.5 MeV. It is expected from these discussions that the most realistic connection of the renormalization factor N_R to the breakup effect must be given by the most realistic folded potential (to be used in the coupled-channels calculation as the bare ^{6}Li+^{12}C potential).

Based on the results of numerous folding analyses [17–19], one might expect that among different folded potentials, the simple M3Y/PP1 potential would give a rather poor agreement with the data, the M3Y/FRE potential (with a more accurate treatment of the exchange term) and finally the DDM3Y1 and BDM3Y1 potentials (with the most sophisticated treatment of the exchange and density-dependent effects) would improve the agreement essentially. It is therefore a surprise to find from Figs. 6–8 and Table I that the M3Y/FRE potential gives no better description than the M3Y/PP1 one, and the DDM3Y1 and BDM3Y1 potentials systematically give a worse description of the data than other simpler versions of the folded potential. A folding analysis [32] using the original DDM3Y interaction [17] also shows that the inclusion of this density dependence into the M3Y/PP1 interaction worsens the fit to the present ^{6}Li+^{12}C scattering data. The M3Y/PP2 potential (with a rather unrealistic treatment of the knock-on exchange effects) gives a description comparable with that given by the M3Y/PP1 potential at $E/A = 10$ and 16.5 MeV only. At higher energies, when the refractive effects become stronger, the M3Y/PP2 potential also gives a poorer description of the data. Since the refractive pattern is sensitive to the real potential at small radii [2], these results indicate that the *renormalized* M3Y/PP2, DDM3Y1, and BDM3Y1 potentials have unrealistic shapes at small internuclear distances. In Figs. 10 and 11 we have plotted radial shapes of different folded potentials before and after renormalization, at $E/A = 16.5$ and 26 MeV, respectively. One finds that the renormalization of the various potentials tends to give about the same value of the real potential

TABLE I. OM parameters [see Eqs. (14) and (15)] used in the folding analysis of the elastic ^{6}Li+^{12}C data at $E_{\rm lab} = 60$, 99, 156, 210, and 318 MeV.

Potential	N_R	$-J_R/6A$ (MeV fm^3)	$\langle r_R^2\rangle^{\frac{1}{2}}$ (fm)	W_V (MeV)	r_V (fm)	a_V (fm)	$-J_W/6A$ (MeV fm^3)	$\langle r_W^2\rangle^{\frac{1}{2}}$ (fm)	σ_R (mb)	χ^2
				^{6}Li+^{12}C, $E_{\rm lab} = 60$ MeV						
M3Y/PP1	0.827	337.6	3.722	29.91	0.876	1.014	144.9	4.682	1487	13.4[a]
M3Y/PP2	0.706	334.0	3.674	30.02	0.876	0.981	141.1	4.585	1431	11.4[a]
M3Y/FRE	0.759	320.0	3.781	53.71	0.614	1.172	160.1	4.747	1606	17.1[a]
DDM3Y1	0.700	276.1	3.880	107.2	0.317	1.260	166.3	4.718	1646	23.1[a]
BDM3Y1	0.718	278.9	3.873	111.2	0.311	1.255	168.2	4.695	1643	22.6[a]
				^{6}Li+^{12}C, $E_{\rm lab} = 99$ MeV						
M3Y/PP1	0.623	248.4	3.730	89.27	0.328	1.328	159.9	4.959	1596	1.4[a]
M3Y/PP2	0.618	248.8	3.727	86.17	0.346	1.321	159.6	4.951	1591	1.3[a]
M3Y/FRE	0.601	243.4	3.790	93.60	0.322	1.321	162.9	4.930	1597	2.7[a]
DDM3Y1	0.630	235.6	3.889	83.61	0.332	1.362	159.5	5.075	1644	9.3[a]
BDM3Y1	0.641	235.9	3.882	85.21	0.330	1.356	160.2	5.052	1637	8.7[a]
				^{6}Li+^{12}C, $E_{\rm lab} = 156$ MeV						
M3Y/PP1	0.744	287.0	3.742	50.31	0.752	0.941	165.9	4.234	1207	8.6
M3Y/PP2	0.933	316.1	3.792	51.36	0.930	0.665	216.0	3.854	1088	14.6
M3Y/FRE	0.742	283.6	3.805	46.99	0.758	0.989	165.4	4.392	1265	8.7
DDM3Y1	0.860	298.2	3.902	54.34	0.948	0.625	234.3	3.808	1077	20.1
BDM3Y1	0.873	297.6	3.896	53.84	0.946	0.631	231.3	3.814	1078	19.5
				^{6}Li+^{12}C, $E_{\rm lab} = 210$ MeV						
M3Y/PP1	0.717	267.8	3.754	93.38	0.525	1.001	173.8	4.063	1128	18.5
M3Y/PP2	0.968	287.7	3.849	75.50	0.850	0.660	252.8	3.650	1020	37.0
M3Y/FRE	0.702	254.4	3.820	140.8	0.396	1.025	183.5	3.985	1131	24.1
DDM3Y1	0.867	279.7	3.916	74.97	0.878	0.630	266.1	3.644	1017	42.8
BDM3Y1	0.879	278.8	3.910	75.32	0.869	0.639	262.0	3.644	1018	41.2
				^{6}Li+^{12}C, $E_{\rm lab} = 318$ MeV						
M3Y/PP1	0.697	243.1	3.781	58.52	0.572	1.142	150.9	4.595	1140	4.9
M3Y/PP2	1.019	243.7	3.960	149.7	0.281	1.153	173.4	4.320	1130	7.1
M3Y/FRE	0.731	238.7	3.853	64.83	0.498	1.208	150.5	4.724	1176	3.2
DDM3Y1	0.871	243.2	3.948	127.9	0.291	1.195	164.9	4.475	1153	6.1
BDM3Y1	0.883	242.4	3.918	126.3	0.292	1.199	164.4	4.488	1155	5.7

[a] χ^2 values obtained with uniform 10% errors.

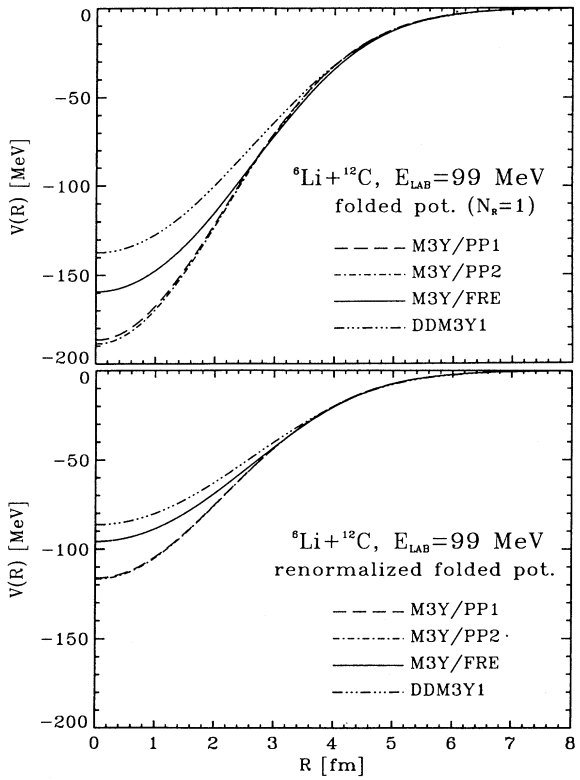

FIG. 10. Unrenormalized (upper part) and renormalized (lower part) by the N_R factors shown in Fig. 9 ^{6}Li+^{12}C folded potentials at $E/A = 16.5$ MeV, generated with the M3Y/PP1, M3Y/PP2, M3Y/FRE, and DDM3Y1 interactions.

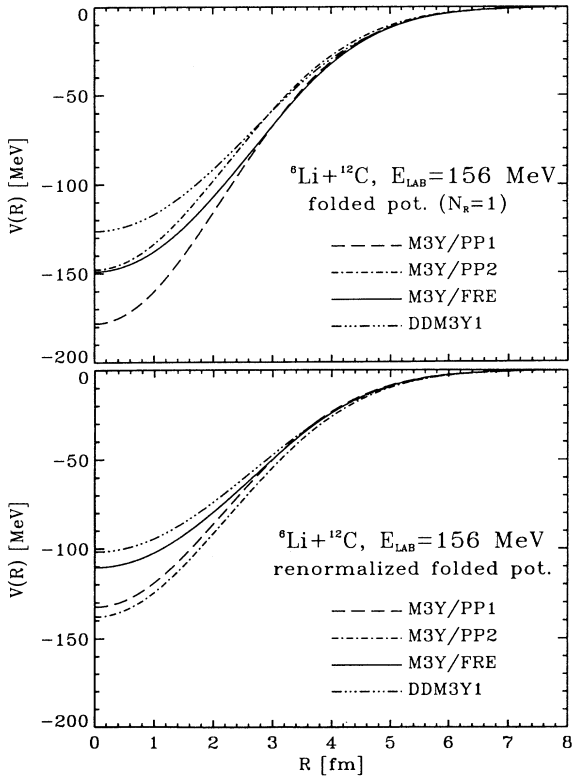

FIG. 11. The same as Fig. 10 but at $E/A = 26$ MeV.

at the surface, around 5 fm. The DDM3Y1 potential becomes too shallow at small radii after being renormalized and this leads to a poorer description of the large angle data. The same behavior is observed with the BDM3Y1 potential, which is close to the DDM3Y1 one. In contrast, the renormalized M3Y/PP2 potential at $E/A = 26$ MeV (and higher energies) becomes deeper than the best-fit (renormalized) M3Y/PP1 potential (Fig. 11) and also gives a worse fit to the data (Figs. 7 and 8). At $E/A = 53$ MeV the refractive part of the angular distribution moves towards smaller angles and the data become less sensitive to the potential at small radii, and all folded potentials give a more or less satisfactory description of the data (Fig. 12).

The fact that the (renormalized) DDM3Y1 and BDM3Y1 potentials give poorer agreement with the data does not necessarily mean that these two density-dependent interactions are unrealistic. Instead, it raises the question whether a simple renormalization ($N_R \neq 1$) of the real folded potential is adequate for ^{6}Li scattering. The theoretical calculations of the breakup [5] indicate that the DPP effects on the optical potential cannot be represented realistically by a simple scaling. Instead, the corresponding DPP contributions to the real potential are peaked in the surface. It is the need to reproduce the correct value of the real potential in the surface that mainly determines the N_R value. But then the renor-

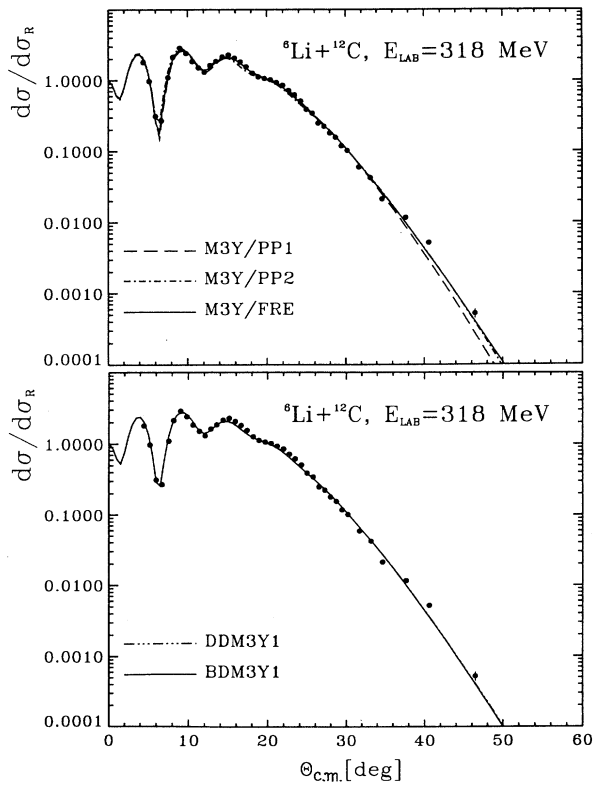

FIG. 12. The same as Fig. 6 but at $E/A = 53$ MeV.

malized potential at small radii is unrealistic, and this deficiency is revealed at those energies where the scattering is sensitive to this radial region. Consequently, we now consider a procedure that takes this into account by using the spline procedure (16).

C. Folding+spline analysis of the ^{6}Li+^{12}C scattering and the effective DPP correction to the real folded potential

The results discussed in the previous section clearly indicate that simply renormalizing the folded potential is not adequate to take into account the breakup effects in the ^{6}Li+^{12}C case. Therefore, we have further analyzed the same data using the definition (16) for the optical potential. The correction $\Delta V(R)$ to the real folded potential is defined by its values at certain radial knots in the surface region 3 fm $< R <$ 10 fm, with a cubic spline interpolation between the knots. The values at the knots, together with the imaginary potential parameters, are then adjusted to optimize the fit to the data. The renormalization factor N_R was kept fixed at unity. The potential values at R outside the spline-search region were fixed to those given by the unrenormalized folded potential. Results obtained in this analysis using different reference folded potentials are shown in Figs. 13–18 and Table II. In general, the fits given by different potentials are much improved (compare the χ^2 values in Tables I and II) due to the more flexible shape of the real potential at the surface. Since the shape of the real potential is fixed at small radii, the difference between different types of the folded potential shows up noticeably in the calculated cross sections at large angles. One finds that the best fit to the data in the whole angular range (at different energies) is given by the OM potentials which use the density-dependent DDM3Y1 and BDM3Y1 potentials as the reference potentials for the spline search of the $\Delta V(R)$. The spline fit always leads to about the same value of the real potential at the surface, around 4–5 fm, which mainly determines the renormalization factor N_R given in Table I (compare Figs. 14 and 16 with Figs. 10 and 11). Without affecting the shape of the folded potential at small radii, the folding+spline analysis offers a unique possibility to test different shapes of the folded potential, as given by different effective NN interactions. At E/A = 53 MeV the bare M3Y/PP1 and M3Y/FRE potentials are too deep in the center compared with the DDM3Y1 one (Fig. 19). Therefore, they introduce oscillations into the angular distribution at large angles (Fig. 18) which are not evident in the measurement (although more complete data in this region would be valu-

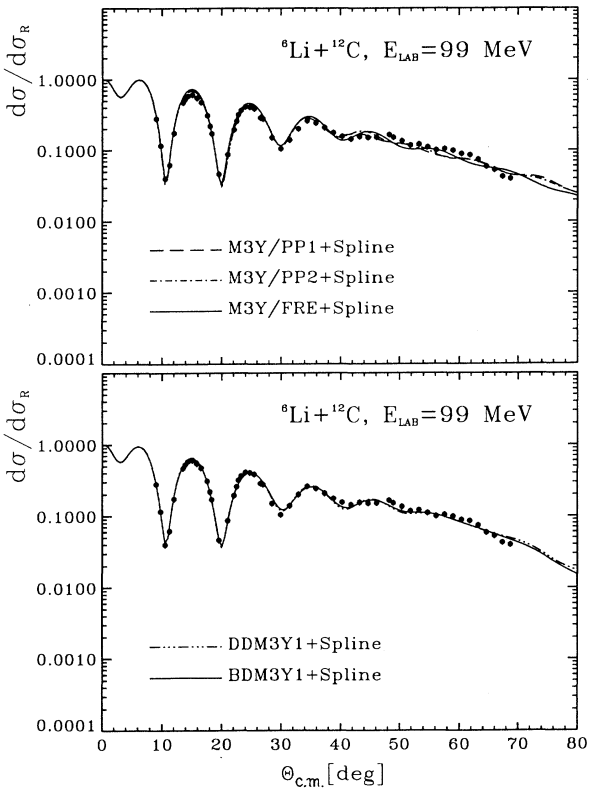

FIG. 13. OM fits to the elastic ^{6}Li+^{12}C scattering data at E/A = 16.5 MeV given by the (unrenormalized) M3Y/PP1, M3Y/PP2, M3Y/FRE (upper part), and DDM3Y1, BDM3Y1 (lower part) folded potentials supplied with a surface spline-shape term. The corresponding OM parameters are given in Table II.

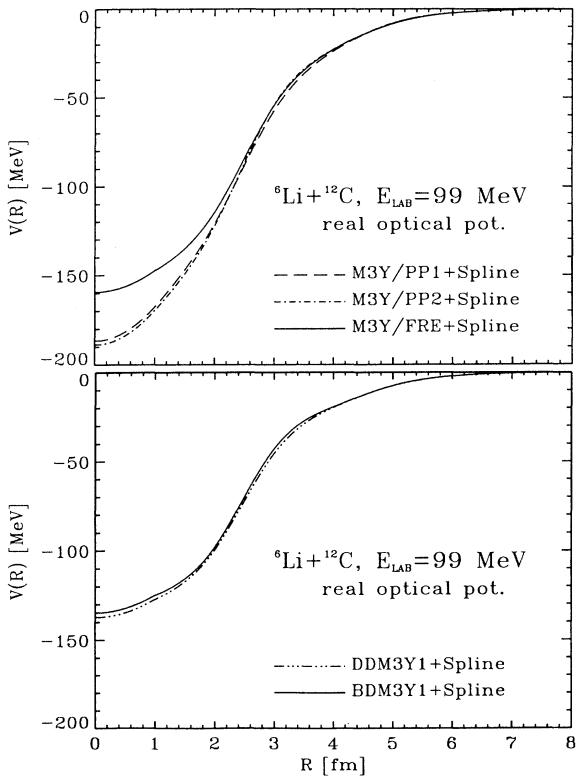

FIG. 14. Unrenormalized M3Y/PP1, M3Y/PP2, M3Y/FRE (upper part), and DDM3Y1, BDM3Y1 (lower part) folded potentials supplied with a surface spline-shape term to fit the elastic scattering data at E/A = 16.5 MeV.

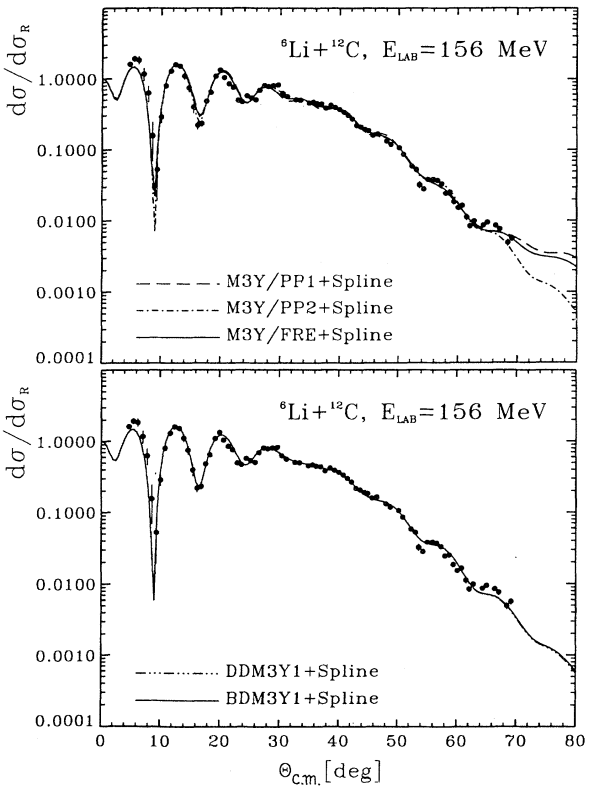

FIG. 15. The same as Fig. 13 but at $E/A = 26$ MeV.

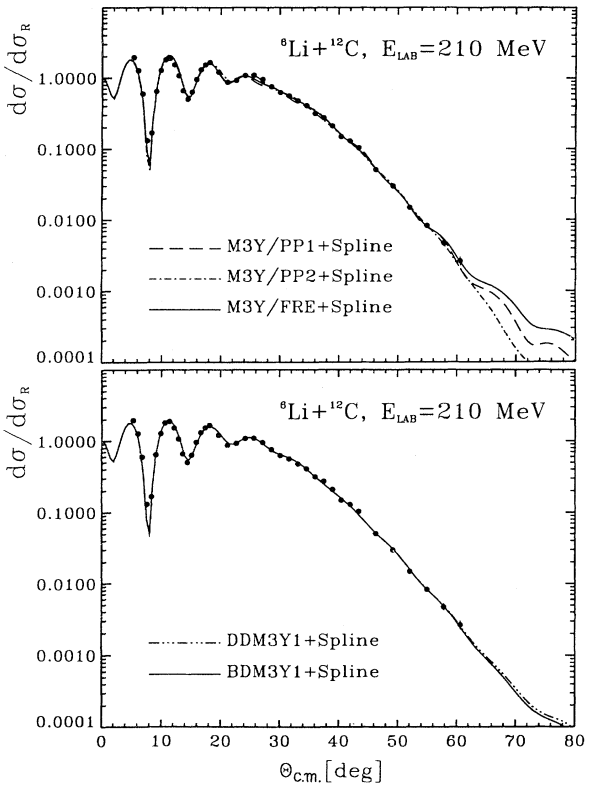

FIG. 17. The same as Fig. 13 but at $E/A = 35$ MeV.

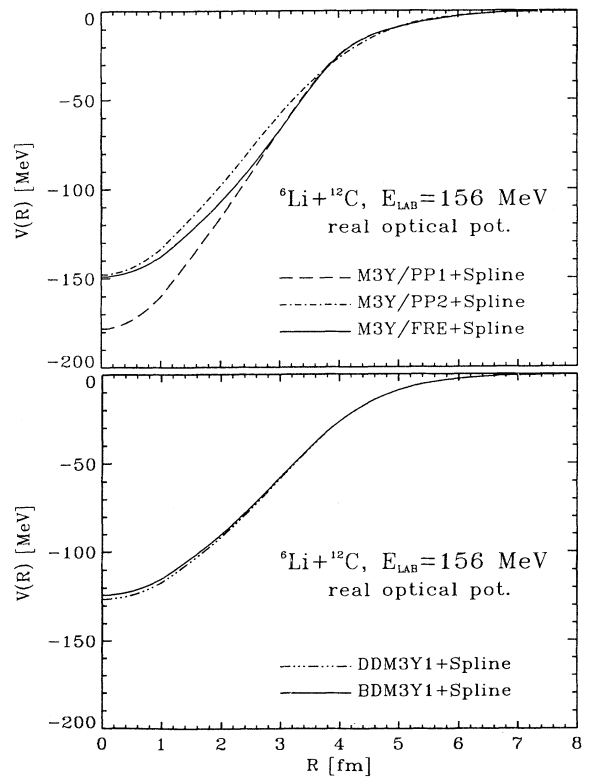

FIG. 16. The same as Fig. 14 but at $E/A = 26$ MeV.

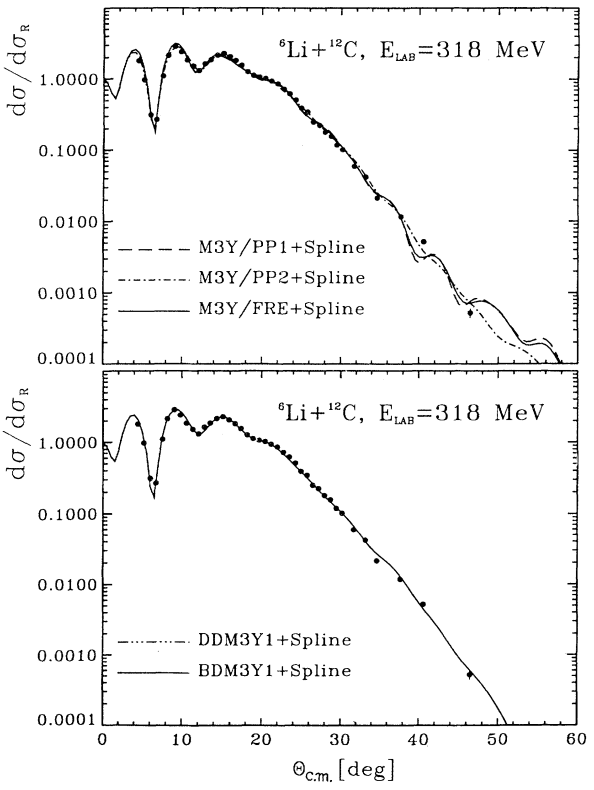

FIG. 18. The same as Fig. 13 but at $E/A = 53$ MeV.

able). The results of the folding+spline analysis now confirm that the DDM3Y1 and BDM3Y1 potentials (with the exchange and density-dependent effects taken properly into account) are the most realistic candidates for the bare ^{6}Li+^{12}C potential, which should be used in an explicit coupled-channels calculation of the breakup process.

As discussed in Sec. III B, the DPP correction $\Delta V(R)$ to the real folded potential due to the breakup effect must depend on the chosen type of the bare folded potential. We emphasize that the $\Delta V(R)$ terms obtained with different folded potentials (see Figs. 14, 16, 20, and 21) are all repulsive and correct the folded potential so that all the real potentials have about the same value at the surface region (R around 4–5 fm) as that given by the renormalization procedure. Therefore, different N_R values obtained with different real folded potentials (Table I) directly indicate different strengths of the DPP term. The energy- and density-dependent DDM3Y1 and BDM3Y1 interactions, which give consistently the best description of the energy dependence of the nucleon optical potential (see Sec. III A) and of the refractive α,^{12}C, and ^{16}O scattering data [10,20], are shown in the present folding+spline analysis also to give the best folded potentials for the bare ^{6}Li+^{12}C system. This gives us the confidence to interpret the surface corrections $\Delta V(R)$ to the DDM3Y1 and BDM3Y1 potentials found at different energies as the DPP contribution caused by the breakup effect. In Figs. 20 and 21 we show the DDM3Y1 potentials [unrenormalized, renormalized to fit the data as shown in Sec. III B, and unrenormalized but with the spline-fit $\Delta V(R)$ term added] at different energies. The $\Delta V(R)$ correction to the bare DDM3Y1 potential, unlike that obtained with the M3Y/PP1 potential, seems to depend more strongly on the incident energy. The effective DPP contribution (Figs. 20 and 21) is strongest at $E/A =$ 16.5 MeV, with $\Delta V(R)/[V_D(R)+V_{EX}(R)] \simeq 40\%$ in the surface. At $E/A = 35$ and 53 MeV this ratio is about 13%. Although the DPP strength is weaker at high energies, its contribution is essential to improve the description of the scattering data (compare, e.g., the lower parts of Figs. 7 and 8 with those of Figs. 15 and 17). The final answer on the energy dependence of the DPP correction might be obtained in a complete coupled-channels calculation [5], using the realistic energy- and density-dependent DDM3Y1 or BDM3Y1 potential as the bare ^{6}Li+^{12}C potential to describe the scattering data at different energies.

TABLE II. OM parameters [see Eq. (16)] used in the folding+spline analysis of the elastic ^{6}Li+^{12}C data at $E_{\rm lab} = 60$, 99, 156, 210, and 318 MeV. $N_R = 1$ for all folded potentials.

Potential	$-J_R/6A$ (MeV fm^3)	$\langle r_R^2\rangle^{\frac{1}{2}}$ (fm)	W_V (MeV)	r_V (fm)	a_V (fm)	$-J_W/6A$ (MeV fm^3)	$\langle r_W^2\rangle^{\frac{1}{2}}$ (fm)	σ_R (mb)	χ^2
			^{6}Li+^{12}C, $E_{\rm lab} = 60$ MeV						
M3Y/PP1+Spline	357.9	3.577	41.22	0.771	1.044	158.4	4.582	1481	11.6[a]
M3Y/PP2+Spline	475.0	3.463	38.48	0.775	1.028	147.0	4.541	1444	8.5[a]
M3Y/FRE+Spline	355.4	3.739	39.22	0.794	1.028	157.1	4.572	1491	12.0[a]
DDM3Y1+Spline	342.3	3.648	37.35	0.806	1.021	153.3	4.573	1463	9.4[a]
BDM3Y1+Spline	342.7	3.651	39.83	0.777	1.036	154.4	4.567	1470	9.5[a]
			^{6}Li+^{12}C, $E_{\rm lab} = 99$ MeV						
M3Y/PP1+Spline	329.9	3.579	168.2	0.284	1.158	198.0	4.338	1462	1.6[a]
M3Y/PP2+Spline	321.2	3.553	147.0	0.291	1.190	187.6	4.455	1483	1.6[a]
M3Y/FRE+Spline	314.3	3.593	167.7	0.285	1.157	197.9	4.337	1461	2.4[a]
DDM3Y1+Spline	273.2	3.630	84.05	0.385	1.281	161.6	4.851	1556	1.1[a]
BDM3Y1+Spline	265.3	3.630	86.93	0.335	1.328	158.3	4.963	1591	0.9[a]
			^{6}Li+^{12}C, $E_{\rm lab} = 156$ MeV						
M3Y/PP1+Spline	357.1	3.714	34.07	1.015	0.640	176.5	4.003	1073	7.9
M3Y/PP2+Spline	323.8	3.716	44.37	0.927	0.714	192.0	3.968	1109	5.0
M3Y/FRE+Spline	346.5	3.740	34.94	1.001	0.657	176.8	4.002	1082	6.2
DDM3Y1+Spline	316.6	3.751	39.84	0.949	0.718	183.0	4.029	1115	4.6
BDM3Y1+Spline	313.2	3.748	39.59	0.948	0.723	182.0	4.038	1118	4.5
			^{6}Li+^{12}C, $E_{\rm lab} = 210$ MeV						
M3Y/PP1+Spline	346.3	3.678	56.65	0.865	0.712	206.3	3.818	1038	11.0
M3Y/PP2+Spline	279.1	3.737	56.65	0.748	0.875	172.3	4.028	1089	10.4
M3Y/FRE+Spline	326.2	3.695	48.19	0.894	0.715	190.8	3.892	1041	9.6
DDM3Y1+Spline	288.7	3.744	42.63	0.857	0.810	165.8	4.062	1071	9.2
BDM3Y1+Spline	285.6	3.748	44.40	0.839	0.824	165.3	4.061	1075	9.5
			^{6}Li+^{12}C, $E_{\rm lab} = 318$ MeV						
M3Y/PP1+Spline	332.6	3.735	65.27	0.910	0.658	258.4	3.787	1013	8.3
M3Y/PP2+Spline	236.7	3.923	121.5	0.296	1.210	163.3	4.530	1163	3.4
M3Y/FRE+Spline	311.4	3.806	59.41	0.921	0.658	242.5	3.815	1006	7.6
DDM3Y1+Spline	262.3	3.869	34.57	0.858	0.947	150.9	4.451	1093	3.3
BDM3Y1+Spline	259.5	3.888	34.15	0.846	0.976	148.4	4.511	1105	2.9

[a] χ^2 values obtained with uniform 10% errors.

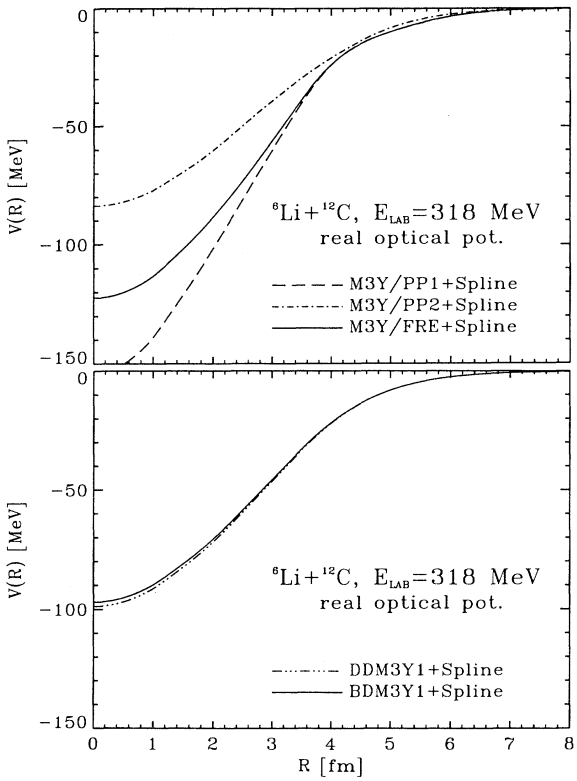

FIG. 19. The same as Fig. 14 but at $E/A = 53$ MeV.

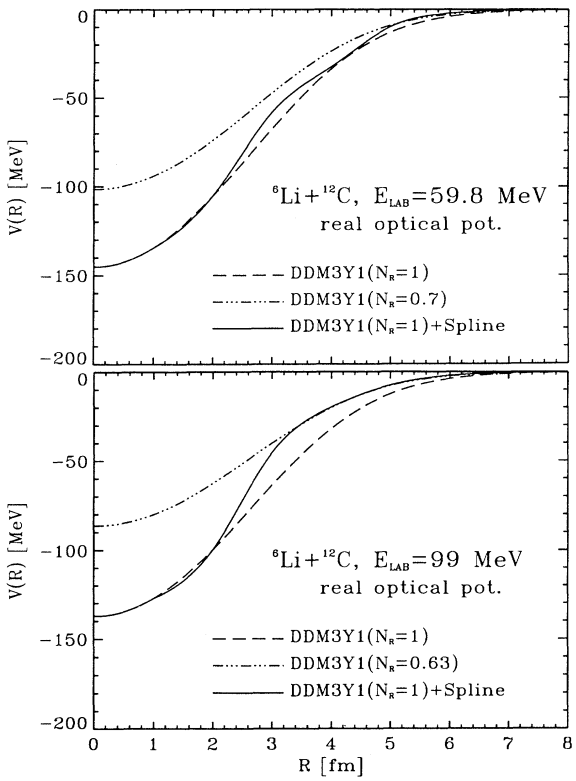

FIG. 20. Unrenormalized, renormalized by the N_R factors shown in Fig. 9 and unrenormalized but supplied with a surface spline-shape term ^{6}Li+^{12}C folded potentials at $E/A = 10$ (upper part) and 16.5 MeV (lower part), generated with the energy- and density-dependent DDM3Y1 interaction.

We show further in Fig. 22 the volume integrals per interacting nucleon pair of the real ($J_R/6A$) and imaginary ($J_W/6A$) parts of the optical potential obtained at different energies in our folding+spline analysis (the $J_R/6A$ values at $E/A = 80$ MeV are just given by the bare folded potentials). Values given by the BDM3Y1 potential are close to those given by the DDM3Y1 potential and are not shown in Fig. 21. One finds that only the DDM3Y1 potential give values close to the empirical trend shown in Fig. 9, while other potentials (even with a spline correction added) give $J_R/6A$ values strongly deviating from it. The WS imaginary potentials obtained with the real DDM3Y1 folded+spline potential seems also to agree with previous OM analyses of these data [6,7], where $J_W/6A$ is found to be centered around -150 MeV fm^3 at all energies.

To be sure that the results of the folding+spline analysis are stable, we have reanalyzed some data using the BDM3Y1 folded+spline potential as the starting real potential in the prescription (14). The results show that the N_R factors obtained are very close to unity and the imaginary potential parameters are close to those in Table II. For example, $N_R = 1.0041$ for the energy 99 MeV where the breakup effect is shown to be strongest. The parameters of the WS imaginary potential obtained at this energy are rather different from other cases which might also give a hint on the DPP effect in the imaginary potential.

Finally we note that a folding+spline analysis involving other density-dependent versions of the M3Y interaction (BDM3Y2 and BDM3Y3), which also reproduce saturation properties of cold nuclear matter but give higher nuclear incompressibilities [10,11], has shown [33] that the best fit to the ^{6}Li+^{12}C scattering data is again obtained with the DDM3Y1 and BDM3Y1 folded potentials. These results confirm a conclusion drawn in our previous folding analyses [10,20] that the most realistic value of the nuclear incompressibility K is around 200 MeV.

IV. SUMMARY

Different versions of the M3Y interaction, with different treatments of the nucleon knock-on exchange effects and of the density dependence, have been used in a study of the energy dependence of the nucleon optical potential as well as in a systematic folding analysis of the elastic ^{6}Li+^{12}C scattering data at $E_{\rm lab}$=60–318 MeV. For the latter, a generalized version [10] of the double-folding model was applied, where the (local) exchange part of the folded potential is evaluated exactly, within a local density formalism.

It is found that the among the two M3Y/PP1 and M3Y/PP2 interactions which use zero-range pseudopotential approximation for the exchange term, the

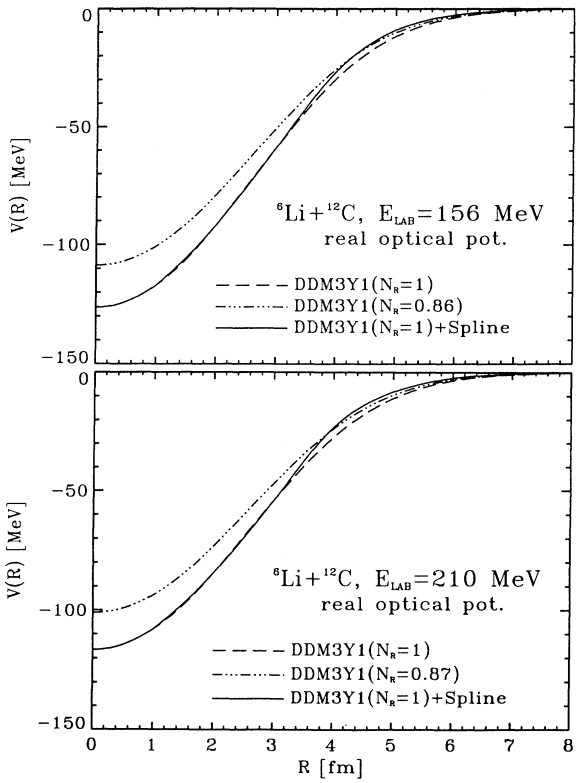

FIG. 21. The same as Fig. 20 but at E/A = 26 (upper part) and 35 MeV (lower part).

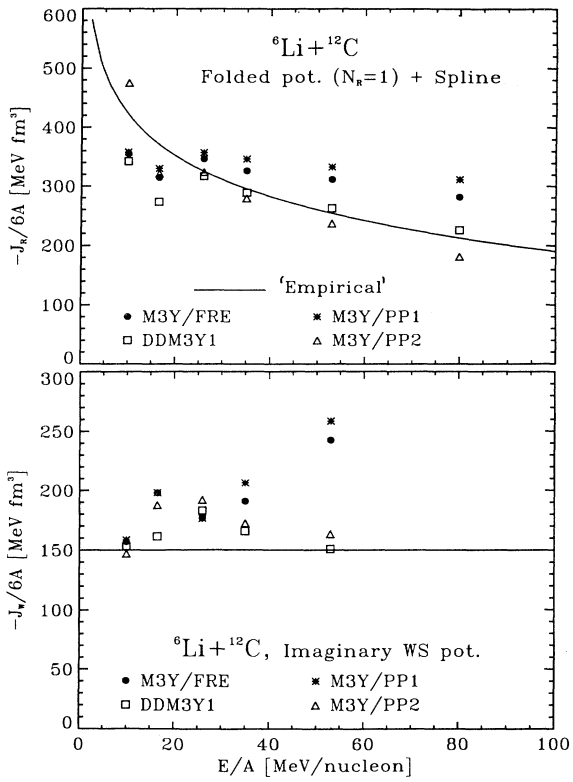

FIG. 22. Energy dependence of the volume integral per interacting nucleon pair of the real ($J_R/6A$) and imaginary ($J_W/6A$) parts of different optical potentials for ^{6}Li+^{12}C, using the real (unrenormalized) folded potentials supplied with a surface spline-shape term. The $J_R/6A$ values at E/A = 80 MeV are taken as given by the bare folded potentials. The solid $J_R/6A$ curve is the "empirical" logarithmic dependence suggested in Refs. [6,7,9].

M3Y/PP1 one produces results closer to those given by a more precise treatment of the exchange effects, i.e., the M3Y/FRE potentials. The energy dependence of the nucleon optical potential, and eventually that of the ^{6}Li+^{12}C optical potential, is shown to be determined mainly by the exchange term which makes a correct treatment of the knock-on exchange effects essential.

Given that the contribution from the DPP to the real part of the ^{6}Li+^{12}C optical potential is strongest at the surface [5] and that the ^{6}Li+^{12}C data are sensitive to the real potential not only at the surface but also at smaller distances, a renormalization of the folded potential as a whole can be misleading. Therefore, the DPP contributions to different real (unrenormalized) folded potentials have been further simulated by a surface correction term, with the shape given by splines. The results of the folding+spline analysis show that different energy dependences of the (effective) DPP contribution to the real folded ^{6}Li+^{12}C potential are found with different types of the folded potential. The energy- and density-dependent DDM3Y1 and BDM3Y1 interactions, which give consistently good description of the nuclear matter properties and the energy dependence of the nucleon optical potential, are shown in the present folding+spline analysis also to be the most successful type of the folded potential for the ^{6}Li+^{12}C system. Thus, the surface corrections $\Delta V(R)$ found with the DDM3Y1 and BDM3Y1 potentials (strongest at $E_{\rm lab}$=99 MeV) might give the most realistic indication of the energy dependence of the DPP caused by the breakup effect.

The success of the DDM3Y1 and BDM3Y1 interactions in the present folding+spline analysis of the ^{6}Li+^{12}C scattering data also confirms the conclusion drawn earlier [10,20] that the best folded potential is that built upon density-dependent interactions, which have parameters chosen to reproduce the saturation properties of nuclear matter and which predict a nuclear incompressibility K around 200 MeV.

ACKNOWLEDGMENTS

We thank M.E. Brandan for helpful communication which stimulated the present study. We are also indebted to A. Nadasen and H.J. Gils for providing us with the tabulated ^{6}Li+^{12}C data. The research was supported, in part, by a grant from the Verbundforschung BMFT of Germany and by the U.S. Department of Energy under Contract No. DE-AC05-84OR21400 managed by Martin Marietta Energy Systems, Inc.

[1] G.R. Satchler and W.G. Love, Phys. Rep. **55**, 183 (1979).
[2] G.R. Satchler, Nucl. Phys. **A409**, 3c (1983).
[3] R.C. Fuller, Phys. Rev. C **12**, 1561 (1975).
[4] G. Bertsch, J. Borysowicz, H. McManus, and W.G. Love, Nucl. Phys. **A284**, 399 (1977).
[5] Y. Sakuragi, Phys. Rev. C **35**, 2161 (1987); Y. Sakuragi, M. Yahiro, and M. Kamimura, Prog. Theor. Phys. Suppl. **89**, 136 (1986).
[6] A. Nadasen, M. McMaster, G. Gunderson, A. Judd, S. Villanueva, P. Schwandt, J.S. Winfield, J. van der Plicht, R.E. Warner, F.D. Becchetti, and J.W. Jänecke, Phys. Rev. C **37**, 132 (1988).
[7] A. Nadasen, T. Stevens, J. Farhat, J. Brusoe, P. Schwandt, J.S. Winfield, G. Yoo, N. Anantaraman, F.D. Becchetti, J. Brown, B. Hotz, J.W. Jänecke, D. Roberts, and R.E. Warner, Phys. Rev. C **47**, 674 (1993).
[8] G.R. Satchler and W.G. Love, Phys. Rev. C **49**, 2254 (1994).
[9] A. Nadasen, J. Winfield, P. Schwandt, J. Farhat, L. Nieman, R.E. Warner, F.D. Becchetti, J.W. Jänecke, and N. Anantaraman, Phys. Rev. C **49**, 2258 (1994).
[10] Dao T. Khoa, W. von Oertzen, and H.G. Bohlen, Phys. Rev. C **49**, 1652 (1994).
[11] Dao T. Khoa and W. von Oertzen, Phys. Lett. B **304**, 8 (1993).
[12] W.G. Love and L.W. Owen, Nucl. Phys. **A239**, 74 (1975).
[13] M. Golin, F. Petrovich, and D. Robson, Phys. Lett. **64B**, 253 (1976).
[14] D.A. Goldberg, S.M. Smith, H.G. Pugh, P.G. Roos, and N.S. Wall, Phys. Rev. C **7**, 1938 (1973); D.A. Goldberg, S.M. Smith, and G.F. Burdzik, *ibid.* **10**, 1362 (1974).
[15] H.G. Bohlen, M.R. Clover, G. Ingold, H. Lettau, and W. von Oertzen, Z. Phys. A **308**, 121 (1982); H.G. Bohlen, X.S. Chen, J.G. Cramer, P. Fröbrich, B. Gebauer, H. Lettau, A. Miczaika, W. von Oertzen, R. Ulrich, and Th. Wilpert, *ibid.* **322**, 241 (1985).
[16] E. Stiliaris, H.G. Bohlen, P. Fröbrich, B. Gebauer, D. Kolbert, W. von Oertzen, M. Wilpert, and Th. Wilpert, Phys. Lett. B **223**, 291 (1989).
[17] A.M. Kobos, B.A. Brown, P.E. Hodgson, G.R. Satchler, and A. Budzanowski, Nucl. Phys. **A384**, 65 (1982); M.E. Brandan and G.R. Satchler, *ibid.* **A487**, 477 (1988).
[18] A.K. Chaudhuri and B. Sinha, Nucl. Phys. **A455**, 169 (1986).
[19] Dao T. Khoa, Nucl. Phys. **A484**, 376 (1988).
[20] Dao T. Khoa and W. von Oertzen, Phys. Lett. B **342**, 6 (1995); Dao T. Khoa, W. von Oertzen, H.G. Bohlen, G. Bartnitzky, H. Clement, Y. Sugiyama, B. Gebauer, A.N. Ostrowski, Th. Wilpert, M. Wilpert, and C. Langner, Phys. Rev. Lett. **74**, 34 (1995).
[21] X. Campi and A. Bouyssy, Phys. Lett. **73B**, 263 (1978).
[22] M. El-Azab Farid and G.R. Satchler, Nucl. Phys. **A438**, 525 (1985).
[23] G.R. Satchler, Nucl. Phys. **A329**, 233 (1979).
[24] M.H. Macfarlane and S.C. Pieper, Argonne National Laboratory Report No. ANL-76-11, 1978 (unpublished).
[25] J.P. Jeukenne, A. Lejeune, and C. Mahaux, Phys. Rep. **25**, 83 (1976); C. Mahaux and R. Sartor, Adv. Nucl. Phys. **20**, 1 (1991).
[26] A. Bohr and B.R. Mottelson, *Nuclear Structure* (Benjamin, New York, 1969), Vol. I, p. 237.
[27] R.L. Varner, W.J. Thompson, T.L. McAbee, E.J. Ludwig, and T.B. Clegg, Phys. Rep. **201**, 57 (1991).
[28] H.G. Bingham, M.L. Halbert, D.C. Hensley, E. Newman, K.W. Kemper, and L.A. Charlton, Phys. Rev. C **11**, 1913 (1975).
[29] P. Schwandt, W.W. Jakobs, M.D. Kaitchuck, P.P. Singh, W.D. Ploughe, F.D. Becchetti, and J.W. Jänecke, Phys. Rev. C **24**, 1522 (1981).
[30] J. Cook, H.J. Gils, H. Rebel, Z. Majka, and H. Klewe-Nebenius, Nucl. Phys. **A388**, 173 (1982); Report No. KfK 3233, Kernforschungszentrum Karlsruhe, 1981 (unpublished).
[31] D.P. Stanley, F. Petrovich, and P. Schwandt, Phys. Rev. C **22**, 1357 (1980).
[32] M.E. Brandan, private communication.
[33] Dao T. Khoa (unpublished).